

Metallic Contact Contributions in Thermal Hall Conductivity Measurements

Hongyu Ma,¹ Xuesong Hu,¹ and Junren Shi^{1,2,*}

¹*International Center for Quantum Materials, Peking University, Beijing 100871, China*

²*Collaborative Innovation Center of Quantum Matter, Beijing 100871, China*

(Dated: August 18, 2025)

We investigate the influence of metallic contacts on thermal Hall measurements. By analyzing typical measurement configurations, we demonstrate that heat currents bypassing through metallic contacts can generate non-negligible thermal Hall signals, even when the actual thermal Hall conductivity of a measured insulator is zero. We show that the effect predicts thermal Hall conductivities that compare favorably with actual experimental observations across a variety of materials, reproducing both their temperature dependencies and magnitudes by assuming effective contact thicknesses on the order of 10^{-2} of sample widths. It even reproduces the subtle differences in temperature dependencies between materials with high and low longitudinal thermal conductivity. Our study suggests the necessity of suppressing the bypass heat currents in thermal Hall measurements, which can be achieved by properly arranging the measurement configurations.

I. INTRODUCTION

Over the past two decades, the measurement of the thermal Hall effect (THE), as an effective means of probing charge-neutral heat carriers in insulators, has received much attention. The effect was first detected in the paramagnetic insulator $\text{Tb}_3\text{Ga}_5\text{O}_{12}$ [1, 2] and has since been measured in various other insulators, including cuprates [3–5], antiferromagnets [6, 7], and multiferroic materials [8].

Recently, many studies have reported the observation of “giant” THE [9–19]. It is generally believed that charge-neutral carriers like phonons only couple weakly with magnetic fields. Therefore, the THE contributed by them is expected to be small. However, in certain materials, such as cuprates [3] and quantum paraelectrics [20, 21], measured thermal Hall conductivities are much larger than expected. More surprisingly, giant thermal Hall conductivities have even been observed in some elemental substances or their simple compounds, such as black phosphorus, Si and SiO_2 [22, 23]. Theoretical efforts have been made to explain these observations. In cuprates, the THE is usually attributed to phonon-spin interactions [4, 5], since spins can couple to magnetic fields directly. For nonmagnetic insulators, studies primarily focus on extrinsic mechanisms involving phonons, such as phonon-domain wall scattering in SrTiO_3 [24], since intrinsic mechanisms, like the phonon Berry curvature contributions from acoustic [25] and optical phonons [26], yield predictions that are at least four orders of magnitude smaller than experimental observations. There is still room for open inquiries into the origin of the effect.

A notable fact is that metallic components are commonly used in recent measurements of the THE. In contrast, early experiments deliberately avoided metallic components to minimize spurious contributions from

conducting electrons [27]. Later studies show that using metals as heat sinks has a negligible effect on the measurements [2, 28]. On the other hand, besides heat sinks, metallic contacts are also widely employed to ensure efficient thermal connections [4, 7, 29–32].

However, employing metallic contacts in THE measurements introduces a potential issue. When a heat current flows through a sample, a portion of the heat current will inevitably enter metallic contacts that are in direct contact with the sample. Under a magnetic field, this bypass heat current can induce a transverse temperature gradient within the metallic contacts, giving rise to spurious thermal Hall signals. Although these contacts are usually much smaller in geometry than the sample and may appear insignificant, their spurious contribution to the measured thermal Hall coefficients is not necessarily negligible, as metals have much larger thermal Hall conductivities than insulators. This naturally raises a question: What is the influence of metallic contacts on the experimental results?

In this paper, we study the influence of metallic contacts on thermal Hall measurements. By analyzing typical measurement configurations, we demonstrate that heat currents bypassing through metallic contacts can generate non-negligible thermal Hall signals, even when the actual thermal Hall conductivity of a measured material is zero. We show that the effect predicts thermal Hall conductivities that compare favorably with actual experimental observations across a variety of materials, reproducing both their temperature dependencies and magnitudes by assuming effective contact thicknesses on the order of 10^{-2} of sample widths. It even reproduces the subtle differences in temperature dependencies between materials with high and low longitudinal thermal conductivity. Our study suggests the necessity of suppressing the bypass heat currents in thermal Hall measurements. Based on the understanding, we discuss how to minimize the influence of metallic contacts by properly arranging the geometric configurations of measurements.

The remainder of the paper is organized as follows. In Sec. II, we analyze the effect of metallic contacts and de-

* junrenshi@pku.edu.cn

rive a formula for predicting the apparent thermal Hall conductivity of a sample with a zero thermal Hall conductivity. In Sec. III, we apply the formula to estimate measured thermal Hall conductivities for various materials and the results are compared with experimental observations. Finally, we summarize our findings and discuss how to minimize the influence of metallic contacts in Sec. IV.

II. METALLIC CONTACT CONTRIBUTIONS

In recent experiments, metallic contacts are widely employed in THE measurements. Two types of contacts are commonly used. The first type involves thin metallic electrodes attached to the sides of a sample, with widths that are typically a fraction of the sample size [20, 29]. The second type consists of fine metallic wires, typically 25 μm or 50 μm in diameter, affixed to the sample surface [2, 4, 7, 23, 28, 30–33]. Silver and gold are the metals most commonly used for these contacts, and silver paste is often utilized for attaching contacts to a sample.

For clarity in theoretical analysis, we consider two simplified configurations illustrated in Fig. 1. The first configuration, referred to as the electrode configuration (Fig. 1(a)), consists of two thin metallic electrodes attached to the sides of the sample. The second configuration, referred to as the wire configuration (Fig. 1(b)), consists of two fine metallic wires affixed to the sample. For simplicity, we assume that the metallic contacts are of the same height as the sample, allowing us to analyze the configurations in two dimensions.

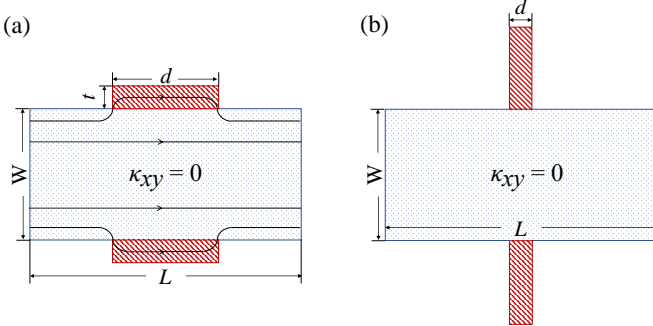


FIG. 1. Simplified schematics of THE measurement configurations. (a) Electrode configuration: The red regions represent metallic electrodes with a thickness t and a width $d \gg t$. The blue region represents the sample to be measured, with a width W and a length L . Arrowed lines illustrate the heat flow through the system as well as that diverted into the electrodes. (b) Wire configuration: The red regions represent metallic wires with a diameter d .

We first analyze the electrode configuration. When a heat current J flows through the sample, a fraction of it enters the electrodes. Since the electrode thickness t is much smaller than its width d , the heat current through them is nearly uniform. Therefore, the electrodes and

sample can be treated as a parallel thermal circuit. The total bypass heat current through the two electrodes can be determined by

$$J_c \approx 2 \frac{\kappa_{xx}^c t}{\kappa_{xx} W + \kappa_{xx}^c t} J \approx 2 \frac{\kappa_{xx}^c}{\kappa_{xx}} \frac{t}{W} J, \quad (1)$$

where κ_{xx} and κ_{xx}^c are the longitudinal thermal conductivities of the sample and the electrodes, respectively, and W is the width of the sample. The bypass heat current in the metallic electrodes induces a transverse temperature difference $\Delta T_y \approx \rho_{xy}^c J_x$, where ρ_{xy}^c denotes the thermal Hall resistivity of the metallic electrodes. In a THE measurement using this configuration, the transverse temperature difference could be misinterpreted as the result of a finite thermal Hall resistivity $\rho_{xy}^{\text{app.}} = \Delta T_y / J$ even if the actual thermal Hall conductivity of the sample is zero. It corresponds to an apparent thermal Hall conductivity:

$$\kappa_{xy}^{\text{app.}} \approx \kappa_{xx}^2 \rho_{xy}^{\text{app.}} \approx 2 \rho_{xy}^c \kappa_{xx}^c \kappa_{xx} \frac{t}{W}. \quad (2)$$

For the wire configuration, the heat current is expected to penetrate the wires over a distance comparable to their diameter d . The approximate heat current distribution within the wires can be determined by solving Fourier's heat equation (see Appendix A). The analysis indicates that a wire has an effective thickness

$$t \approx 0.27d. \quad (3)$$

Eq. (2) can then be applied to determine the apparent thermal Hall conductivity.

For simplicity, approximations were made in the preceding analyses. A more realistic analysis based on finite-element simulations, presented in Appendix B, reveals that there exists a geometric correction that depends on the geometric parameter t/d and the ratio $\kappa_{xx}/\kappa_{xx}^c$. With the correction, Eq. (2) is modified as follows:

$$\kappa_{xy}^{\text{app.}} = 2 \rho_{xy}^c \kappa_{xx}^c \kappa_{xx} \frac{t}{W} \delta \left(\frac{t}{d}, \frac{\kappa_{xx}}{\kappa_{xx}^c} \right), \quad (4)$$

where $\delta(t/d, \kappa_{xx}/\kappa_{xx}^c)$ represents the correction factor, and can be well approximated by the Padé formula

$$\delta(p, q) = \frac{(\alpha + p)q}{\beta p + (\alpha + p)q}, \quad (5)$$

with $p \equiv t/d$, $q \equiv \kappa_{xx}/\kappa_{xx}^c$, and the parameters $\alpha = 0.355$, $\beta = 0.694$. The wire configuration corresponds to $t/d \rightarrow \infty$. The correction factor could deviate significantly from unity when $\kappa_{xx}/\kappa_{xx}^c$ is small.

We note that actual geometric configurations in experiments may differ in details from the simplified configurations considered here. Therefore, when applying the formulas, the geometric parameters should be treated as effective ones, adjusted to the actual experimental setup. For instance, in electrode configurations, electrodes often covers a portion of the top and bottom surfaces of

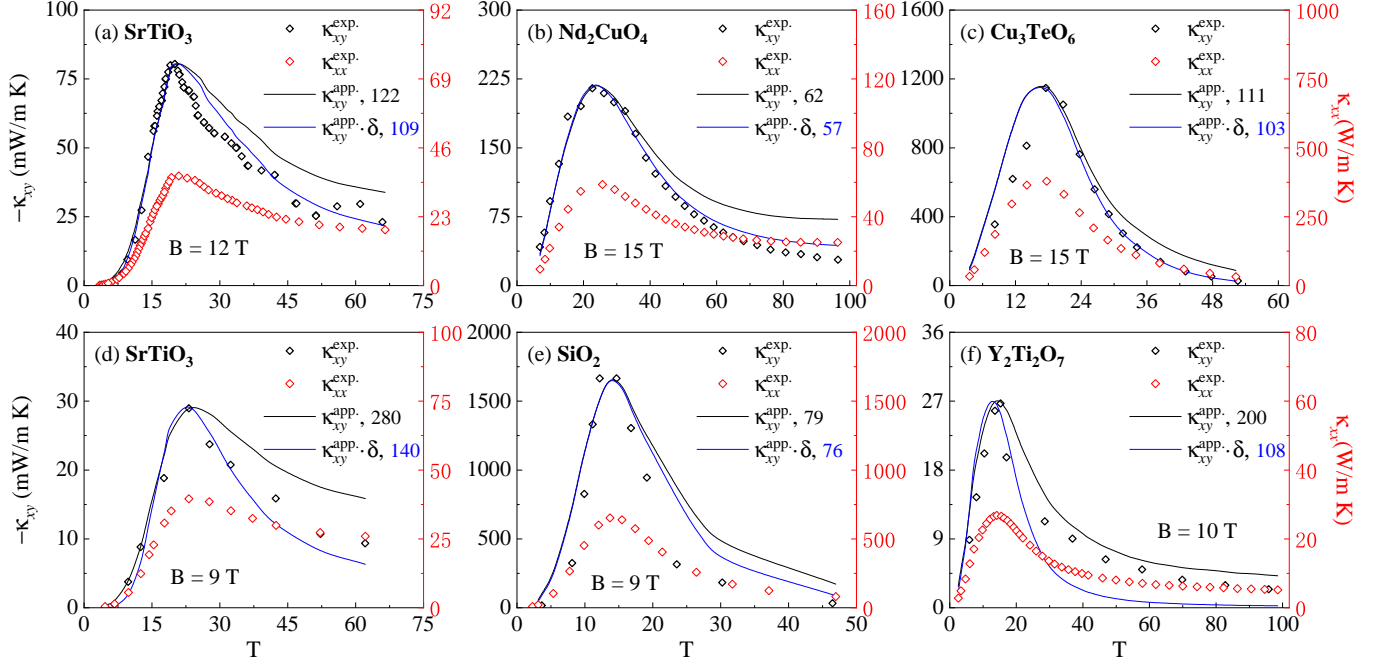


FIG. 2. Fits to experimental thermal Hall conductivity ($\kappa_{xy}^{\text{exp.}}$) for (a) SrTiO₃ [20], (b) Nd₂CuO₄ [5], (c) Cu₃TeO₆ [7], (d) SrTiO₃ [23], (e) SiO₂ [23] and (f) Y₂Ti₂O₇ [34]. Both $\kappa_{xy}^{\text{exp.}}$ and the corresponding longitudinal thermal conductivity ($\kappa_{xx}^{\text{exp.}}$) are adapted from the respective references. Solid curves show fits to $\kappa_{xy}^{\text{exp.}}$, with ($\kappa_{xy}^{\text{app.}} \cdot \delta$) and without ($\kappa_{xy}^{\text{app.}}$) the geometric correction, using Eq. (4) and Eq. (2), respectively. For geometric corrections, (a) and (b) assume the electrode configuration with $t/d = 1/20$, while (c) to (f) assume the wire configuration. Numbers adjacent to the legends indicate the W/t values used for fitting.

the sample. Its effect can be approximated by scaling the thickness t by a factor according to the increased total area of the electrode. For more accurate estimates, one can always consider the actual contact geometry and employ finite-element simulations.

III. FIT TO EXPERIMENTAL RESULTS

To evaluate the significance of metallic contact contributions in THE measurements, we fit experimental data from various materials obtained by different experimental groups using Eq. (2) and Eq. (4) under the assumption that the actual thermal Hall conductivities of the samples are zero. We fit the experimentally measured κ_{xy} - T relations simply by aligning their peak values with those of $\kappa_{xy}^{\text{app.}}$ determined using Eq. (2) or Eq. (4). These fits yield nominal values for the geometric parameter W/t . By assessing whether these geometric parameters fall within a realistic range, one can judge the relevance of metallic contact contributions to THE measurements.

To facilitate the fitting, we need to assume a set of parameters, as their actual values vary across different experiments and are not always available. The thermal conductivity κ_{xy}^c and the thermal Hall resistivity ρ_{xy}^c of the metallic contacts are derived from their electrical conductivity and Hall resistivity using the Wiedemann-Franz law [35]. The electrical conductivity of the metallic con-

tacts is set to 10^8 S/m, an intermediate value between those of silver paste and silver. The temperature dependent electric Hall coefficient R_H is taken from silver [36]. For the longitudinal thermal conductivity of the sample, κ_{xx} , we use actual measurement data usually reported alongside thermal Hall results. Although these values may not match the actual ones in experiments, the difference can always be compensated by scaling the geometric parameter W/t . Thus, the fitted geometric parameters should be treated as nominal.

Fits to a few representative experimental results from different studies are presented in Fig. 2. The black and blue curves correspond to fits performed without and with the geometric correction, respectively. The geometric parameter W/t used in each fit is indicated in the legend.

It can be seen, above all, that the contact contribution $\kappa_{xy}^{\text{app.}}$ reproduces the correct sign of the experimentally observed thermal Hall conductivity $\kappa_{xy}^{\text{exp.}}$. Experimental data exhibit a curious skewed distribution of $\kappa_{xy}^{\text{exp.}}$ values, most of which are measured negative. This happens to match the sign of the contact contribution, as the Hall coefficients of metals commonly used in contacts, such as Au and Ag, are all negative.

Furthermore, $\kappa_{xy}^{\text{app.}}$ exhibits temperature dependencies similar to those of $\kappa_{xy}^{\text{exp.}}$, with closely aligned peak temperatures. Incorporating the geometric correction improves the quantitative agreement between $\kappa_{xy}^{\text{app.}}$ and

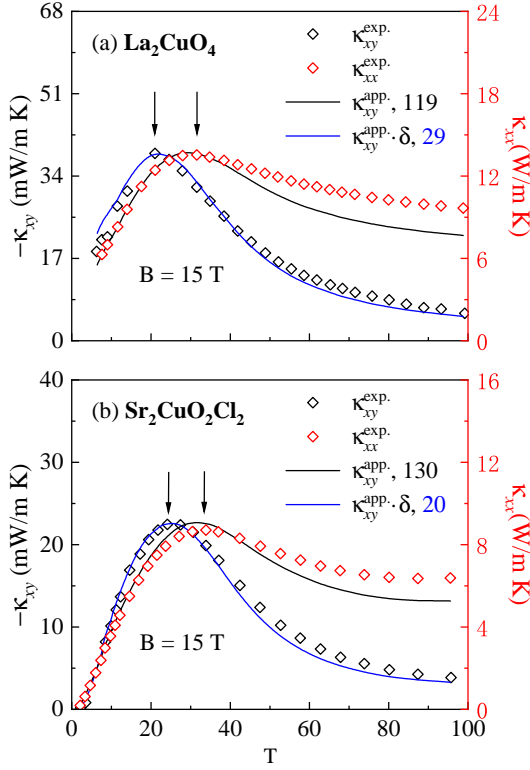


FIG. 3. Same as Fig. 2 but for (a) La_2CuO_4 [5] and (b) $\text{Sr}_2\text{CuO}_2\text{Cl}_2$ [5]. Arrows indicate the peak positions of $\kappa_{xx}^{\text{exp.}}$ and $\kappa_{xy}^{\text{exp.}}$. The wire configuration is assumed when determining geometric corrections.

$\kappa_{xy}^{\text{exp.}}$. According to Eq. (2), the contact contribution is proportional to κ_{xx} , implying that the peak temperature of $\kappa_{xy}^{\text{app.}}$ coincides with that of κ_{xx} . This is indeed observed in the experimental data shown in Fig. 2.

On the other hand, certain materials deviate from this behavior, exhibiting peak temperatures of $\kappa_{xy}^{\text{exp.}}$ lower than those of κ_{xx} , as evident in Fig. 3 for La_2CuO_4 and $\text{Sr}_2\text{CuO}_2\text{Cl}_2$. Compared to the materials shown in Fig. 2, these materials have smaller κ_{xx} , falling in the regime where the geometric correction becomes significant. Remarkably, after incorporating the geometric correction, the contact contribution $\kappa_{xy}^{\text{app.}}$ reproduces the observed shift of the peak temperatures, as shown in Fig. 3.

The nominal values of W/t required to reproduce the magnitudes of the experimental data range from 20 to 280, depending on the material and experiments. Variations between experiments for the same material, such as SrTiO_3 in Fig. 2(a) and (d), could be attributed to differences in experimental configurations. These values provide a basis for assessing the relevance of contact contributions in specific experiments.

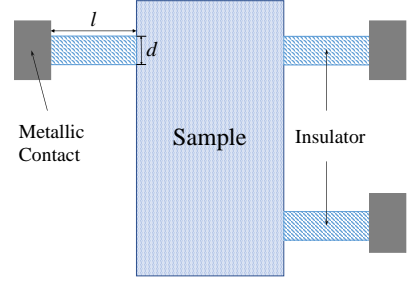


FIG. 4. Simplified schematic of a THE measurement configuration designed to suppress bypass heat currents. Contacts between the sample and metallic components should be buffered by long insulating strips with $l \gg d$.

IV. SUMMARY AND DISCUSSION

In summary, we investigate the influence of metallic contacts on THE measurements. Our analysis shows that metallic contacts, even with geometric dimensions much smaller than insulating samples, can induce a sizable thermal Hall conductivity. Fits assuming THE arises solely from metallic contacts seem to reproduce the overall trends observed in experiments and account for sample-to-sample variations.

Our analysis indicates that suppressing bypass heat currents is critical for minimizing the influence of metallic contacts on thermal Hall conductivity measurements. Direct contact between a sample and metallic components must be avoided. Figure 4 illustrates a configuration designed to suppress bypass heat currents. As analyzed in Appendix B, the heat current within a wire decays exponentially along its length direction. Therefore, using insulating wires that are THE inert and have lengths greater than their diameters can effectively suppress bypass heat currents into metallic contacts. A suppression factor of 10^{-4} can be achieved with $l \approx 3d$, where l and d denote the length and diameter of the insulating wires, respectively.

ACKNOWLEDGMENTS

We acknowledge Zengwei Zhu, Shiyang Li, Jian Wang, and Xi Lin for valuable discussions. This work is supported by the National Key R&D Program of China under Grant No. 2021YFA1401900 and the National Science Foundation of China under Grant No. 12174005.

Appendix A: Heat current distribution in a wire

To determine the bypass heat current entering a metallic wire connected to the sample, we consider an infinite wire extending along the y -axis from the origin to infinity, and occupying $x \in [0, d]$. The temperature distribution can be determined by solving Fourier's heat equa-

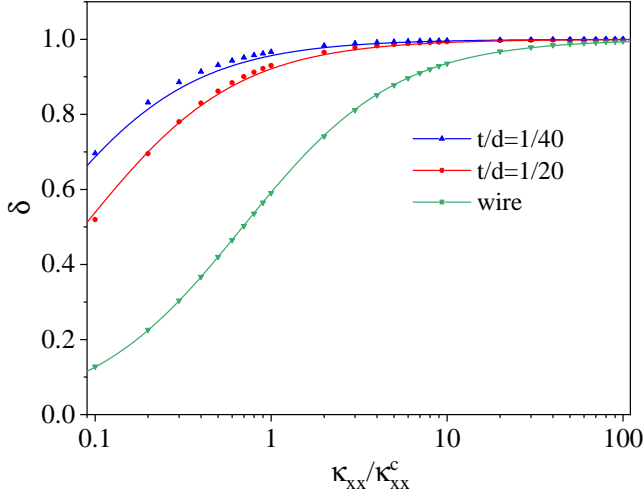


FIG. 5. Geometric correction factor δ as a function of $\kappa_{xx}/\kappa_{xx}^c$ and geometric ratio t/d . Points represent numerical results, while curves show values yielded by the Padé formula Eq. (5). The wire configuration corresponds to $t/d \rightarrow \infty$.

tion $\nabla^2 T = 0$. Assuming adiabatic boundary conditions at the lateral edges of the wire, the general solution takes the form

$$T(x, y) = T_0 + \sum_n A_n e^{-\frac{n\pi}{d}y} \cos\left(\frac{n\pi}{d}x\right), \quad (\text{A1})$$

where A_n are coefficients to be determined. At $y = 0$, we assume that the temperature varies linearly, with a gradient matching that in the bulk of the sample: $T(x, y = 0) = T_0 + [J/(\kappa_{xx}W)]x$. Applying the boundary condition gives:

$$A_n = -\frac{4d}{n^2\pi^2\kappa_{xx}W}J. \quad (\text{A2})$$

The bypass heat current density can be obtained using Fourier's law $j_x = -\kappa_{xx}^c \partial_x T$. The total bypass heat

current along the x -direction, averaged over constant x cross-sections, is given by

$$J_c = 2 \sum_{n \in \text{odd}} \frac{8\kappa_{xx}^c d}{n^3 \pi^3 \kappa_{xx} W} J = 2 \frac{\kappa_{xx}^c}{\kappa_{xx}} \frac{7\zeta(3)}{\pi^3} \frac{d}{W} J \quad (\text{A3})$$

where the factor of 2 accounts for two wires connected to the sample, and $\zeta(x)$ denotes the Riemann zeta function. By comparing Eq. (A3) with Eq. (1) and noting $7\zeta(3)/\pi^3 \approx 0.27$, we deduce the effective thickness for wires with a diameter d , as specified in Eq. (3).

Appendix B: Geometric correction

To evaluate the geometric corrections to Eq. (2), we perform finite element simulations using the heat transfer module in COMSOL for the configurations shown in Fig. 1. For all simulations, we fix $L/W = 2$ and $d/W = 0.4$. Our calculations indicate that the results are nearly independent of d/W when $d/W \lesssim 1$. For the electrode configuration, we vary t/d between 1/20 and 1/40. For the wire configuration, we set $t/d = 50$. A fixed temperature difference is applied across the two ends of the sample along its length, while all other boundaries are treated as adiabatic. Grid density is adjusted to ensure numerical convergence. A typical simulation employs approximately 2×10^6 grid points, with around 10^4 allocated to the metallic contact. In the electrode configuration, the total heat current passing through the center cross-section of the electrodes was computed. For the wire configuration, we evaluated the average heat current in the wires. The geometric correction factor δ is determined as the ratio of the numerical result to the approximate value yielded by Eq. (1).

Figure 5 shows the dependence of the correction factor δ on $\kappa_{xx}/\kappa_{xx}^c$ for various contact geometries. Significant geometric corrections are observed when $\kappa_{xx}/\kappa_{xx}^c \lesssim 1$. The correction is well approximated by the Padé formula Eq. (5).

-
- [1] C. Strohm, G. L. J. A. Rikken, and P. Wyder, Phenomenological evidence for the phonon hall effect, *Phys. Rev. Lett.* **95**, 155901 (2005).
 - [2] A. V. Inyushkin and A. N. Taldenkov, On the phonon hall effect in a paramagnetic dielectric, *JETP Lett.* **86**, 379 (2007).
 - [3] G. Grissonnanche, A. Legros, S. Badoux, E. Lefrançois, V. Zlatko, M. Lizaie, F. Laliberté, A. Gourgout, J.-S. Zhou, S. Pyon, *et al.*, Giant thermal hall conductivity in the pseudogap phase of cuprate superconductors, *Nature* **571**, 376 (2019).
 - [4] G. Grissonnanche, S. Thériault, A. Gourgout, M.-E. Boulanger, E. Lefrançois, A. Ataei, F. Laliberté, M. Dion, J.-S. Zhou, S. Pyon, *et al.*, Chiral phonons in the pseudogap phase of cuprates, *Nature Physics* **16**, 1108 (2020).
 - [5] M.-E. Boulanger, G. Grissonnanche, S. Badoux, A. Lilaire, É. Lefrançois, A. Legros, A. Gourgout, M. Dion, C. Wang, X. Chen, *et al.*, Thermal hall conductivity in the cuprate mott insulators Nd_2CuO_4 and $\text{Sr}_2\text{CuO}_2\text{Cl}_2$, *Nature communications* **11**, 5325 (2020).
 - [6] Y. Onose, T. Ideue, H. Katsura, Y. Shiomi, N. Nagaosa, and Y. Tokura, Observation of the magnon hall effect, *Science* **329**, 297 (2010).
 - [7] L. Chen, M.-E. Boulanger, Z.-C. Wang, F. Tafti, and L. Taillefer, Large phonon thermal Hall conductivity in the antiferromagnetic insulator Cu_3TeO_6 , *Proceedings of the National Academy of Sciences* **119**, e2208016119 (2022).
 - [8] T. Ideue, T. Kurumaji, S. Ishiwata, and Y. Tokura, Giant thermal hall effect in multiferroics, *Nature materials* **16**, 797 (2017).
 - [9] M. Akazawa, M. Shimozaawa, S. Kittaka, T. Sakakibara,

- R. Okuma, Z. Hiroi, H.-Y. Lee, N. Kawashima, J. H. Han, and M. Yamashita, Thermal hall effects of spins and phonons in kagome antiferromagnet cd-kapellasite, *Phys. Rev. X* **10**, 041059 (2020).
- [10] H. Zhang, C. Xu, C. Carnahan, M. Sretenovic, N. Suri, D. Xiao, and X. Ke, Anomalous thermal hall effect in an insulating van der waals magnet, *Phys. Rev. Lett.* **127**, 247202 (2021).
- [11] C. Xu, C. Carnahan, H. Zhang, M. Sretenovic, P. Zhang, D. Xiao, and X. Ke, Thermal hall effect in a van der waals triangular magnet FeCl_2 , *Phys. Rev. B* **107**, L060404 (2023).
- [12] M. Gillig, X. Hong, C. Wellm, V. Kataev, W. Yao, Y. Li, B. Büchner, and C. Hess, Phononic-magnetic dichotomy of the thermal hall effect in the kitaev material $\text{Na}_2\text{Co}_2\text{TeO}_6$, *Phys. Rev. Res.* **5**, 043110 (2023).
- [13] A. Ataei, G. Grissonnanche, M.-E. Boulanger, L. Chen, É. Lefrançois, V. Brouet, and L. Taillefer, Phonon chirality from impurity scattering in the antiferromagnetic phase of Sr_2IrO_4 , *Nature Physics* **20**, 585 (2024).
- [14] Y. Hirokane, Y. Nii, Y. Tomioka, and Y. Onose, Phononic thermal hall effect in diluted terbium oxides, *Phys. Rev. B* **99**, 134419 (2019).
- [15] H.-L. Kim, T. Saito, H. Yang, H. Ishizuka, M. J. Coak, J. H. Lee, H. Sim, Y. S. Oh, N. Nagaosa, and J.-G. Park, Thermal hall effects due to topological spin fluctuations in YMnO_3 , *Nature Communications* **15**, 243 (2024).
- [16] E. Lefrançois, G. Grissonnanche, J. Baglo, P. Lampen-Kelley, J.-Q. Yan, C. Balz, D. Mandrus, S. E. Nagler, S. Kim, Y.-J. Kim, N. Doiron-Leyraud, and L. Taillefer, Evidence of a phonon hall effect in the kitaev spin liquid candidate $\alpha\text{-RuCl}_3$, *Phys. Rev. X* **12**, 021025 (2022).
- [17] B. Flebus and A. H. MacDonald, Charged defects and phonon hall effects in ionic crystals, *Phys. Rev. B* **105**, L220301 (2022).
- [18] K. Sugii, M. Shimozawa, D. Watanabe, Y. Suzuki, M. Halim, M. Kimata, Y. Matsumoto, S. Nakatsuji, and M. Yamashita, Thermal hall effect in a phonon-glass $\text{Ba}_3\text{CuSb}_2\text{O}_9$, *Phys. Rev. Lett.* **118**, 145902 (2017).
- [19] M. Nawwar, R. R. Neumann, J. Wen, A. Mook, I. Mertig, and J. P. Heremans, Large thermal hall effect in MnPS_3 , *arXiv preprint arXiv:2503.11639* (2025).
- [20] X. Li, B. Fauqué, Z. Zhu, and K. Behnia, Phonon thermal hall effect in strontium titanate, *Phys. Rev. Lett.* **124**, 105901 (2020).
- [21] S. Sim, H. Yang, H.-L. Kim, M. J. Coak, M. Itoh, Y. Noda, and J.-G. Park, Sizable suppression of thermal hall effect upon isotopic substitution in SrTiO_3 , *Phys. Rev. Lett.* **126**, 015901 (2021).
- [22] X. Li, Y. Machida, A. Subedi, Z. Zhu, L. Li, and K. Behnia, The phonon thermal hall angle in black phosphorus, *Nature Communications* **14**, 1027 (2023).
- [23] X. Jin, X. Zhang, W. Wan, H. Wang, Y. Jiao, and S. Li, Discovery of universal phonon thermal hall effect in crystals, *arXiv preprint arXiv:2404.02863* (2024).
- [24] J.-Y. Chen, S. A. Kivelson, and X.-Q. Sun, Enhanced thermal hall effect in nearly ferroelectric insulators, *Phys. Rev. Lett.* **124**, 167601 (2020).
- [25] T. Qin, J. Zhou, and J. Shi, Berry curvature and the phonon hall effect, *Phys. Rev. B* **86**, 104305 (2012).
- [26] X. Hu and J. Shi, Intrinsic thermal hall effect of optical phonons enhanced by discrete rotational symmetry, *Phys. Rev. B* **111**, 214303 (2025).
- [27] C. Strohm, *Magneto-transverse Phonon Transport*, Ph.D. thesis, Universität Konstanz, Konstanz (2003).
- [28] M. Hirschberger, J. W. Krizan, R. Cava, and N. Ong, Large thermal hall conductivity of neutral spin excitations in a frustrated quantum magnet, *Science* **348**, 106 (2015).
- [29] S. Jiang, X. Li, B. Fauqué, and K. Behnia, Phonon drag thermal hall effect in metallic strontium titanate, *Proceedings of the National Academy of Sciences* **119**, e2201975119 (2022).
- [30] M.-E. Boulanger, G. Grissonnanche, E. Lefrançois, A. Gourgout, K.-J. Xu, Z.-X. Shen, R. L. Greene, and L. Taillefer, Thermal hall conductivity of electron-doped cuprates, *Phys. Rev. B* **105**, 115101 (2022).
- [31] R. Sharma, M. Bagchi, Y. Wang, Y. Ando, and T. Lorenz, Phonon thermal hall effect in charge-compensated topological insulators, *Phys. Rev. B* **109**, 104304 (2024).
- [32] T. Uehara, T. Ohtsuki, M. Udagawa, S. Nakatsuji, and Y. Machida, Phonon thermal hall effect in a metallic spin ice, *Nature Communications* **13**, 4604 (2022).
- [33] H.-L. Kim, M. J. Coak, J. Baglo, K. Murphy, R. Hill, M. Sutherland, M. C. Hatnean, G. Balakrishnan, and J.-G. Park, Modular thermal hall effect measurement setup for fast-turnaround screening of materials over wide temperature range using capacitive thermometry, *Review of scientific instruments* **90** (2019).
- [34] R. Sharma, M. Valldor, and T. Lorenz, Phonon thermal hall effect in nonmagnetic $\text{Y}_2\text{Ti}_2\text{O}_7$, *Phys. Rev. B* **110**, L100301 (2024).
- [35] N. Ashcroft and N. Mermin, *Solid State Physics* (Cengage Learning, 2022).
- [36] D. R. Smith and F. Fickett, Low-temperature properties of silver, *Journal of research of the National Institute of Standards and Technology* **100**, 119 (1995).